

Application of Kalman Filter to Estimate Junction Temperature in IGBT Power Modules

Mohd. Amir Eleffendi and C. Mark Johnson, *Member, IEEE*

Abstract—Knowledge of instantaneous junction temperature is essential for effective health management of power converters, enabling safe operation of the power semiconductors under all operating conditions. Methods based on fixed thermal models are typically unable to compensate for degradation of the thermal path resulting from aging and the effect of variable cooling conditions. Thermosensitive electrical parameters (TSEPs), on the other hand, can give an estimate of junction temperature T_J , but measurement inaccuracies and the masking effect of varying operating conditions can corrupt the estimate. This paper presents a robust and noninvasive real-time estimate of junction temperature that can provide enhanced accuracy under all operating and cooling conditions when compared to model-based or TSEP-based methods alone. The proposed method uses a Kalman filter to fuse the advantages of model-based estimates and an online measurement of TSEPs. Junction temperature measurements are obtained from an online measurement of the on-state voltage, $V_{CE(ON)}$, at high current and processed by a Kalman filter, which implements a predict-correct mechanism to generate an adaptive estimate of T_J . It is shown that the residual signal from the Kalman filter may be used to detect changes in thermal model parameters, thus allowing the assessment of thermal path degradation. The algorithm is implemented on a full-bridge inverter and the results verified with an IR camera.

Index Terms—Health management, insulated gate bipolar transistors (IGBT), junction temperature, Kalman filter, real time, solder fatigue, thermosensitive electrical parameters (TSEPs).

I. INTRODUCTION

POWER converters that use insulated gate bipolar transistors (IGBT) modules are becoming more common in automotive and rail-traction applications where the combination of environmental and load-derived thermal cycling can result in large and unpredictable fluctuations in junction temperature [1]. In renewable energy applications, the unpredictable mission profiles again result in large amplitude temperature cycles; for example, in the case of wind power turbines, thermal cycles emerge from variations of wind speed [2]. In such conditions, the need for the knowledge of junction temperature becomes vital. In addition, there is a tradeoff between converter size and its heat transfer capabilities. Smaller sizes are desirable for reduced cost but

have increased susceptibility to thermal cycling. Therefore, the knowledge of junction temperature becomes more important.

Accurate knowledge of junction temperature plays a major role in the control and health management algorithms, which have been recently proposed to monitor and extend the reliability of IGBT power modules under in-service conditions. Methods for implementing real-time health management for applications with uncertain mission profiles have been demonstrated [3], [4]. These methods rely on estimates of the junction temperature profile and cycle-counting algorithms to yield equivalent thermal cycle parameters, which are then applied to lifetime reliability models.

Similarly, junction temperature can be used in the active thermal management algorithms to reduce the effects of thermal cycling in power modules and to improve reliability. Power dissipation can be controlled through regulating the current limit, switching frequency and dc-link voltage in a way that limits temperature variations [5]–[7]. Dynamic cooling of power modules is another way to reduce temperature variations [8].

Real-time knowledge of junction temperature is vital for condition monitoring and prognostics of power converter since it can facilitate the identification of competing wear-out mechanisms [9]. For example, in cases, where wire-bond lift-off and solder fatigue happen simultaneously, it is not clear whether changes in the on-state voltage are due to an increase in electrical resistance (wire bond lift) or an increase in thermal resistance (solder fatigue leading to increased temperature and changes in voltage). Therefore, knowledge of junction temperature is essential to discriminate between the thermal aging effects and the wire-bond failures [3]. According to [10], the accuracy of the junction temperature estimate should be within 1 °C for successful application in condition monitoring. In addition, it is suggested in [11] that a continuous monitoring of junction temperature as a failure indicator is required to enable effective IGBT prognostics. An example of IGBT prognostic where junction temperature is required can be found in [12].

One way to obtain an online measurement of IGBT temperature is via integrated sensors. Two types of sensors are typically integrated into power modules, NTC resistors, and on-chip diodes. While NTC resistors are fixed on the DBC substrate and return baseplate temperature with a time constant in the range of few seconds [13], on-chip diodes are integrated within the IGBT chip itself and return the local chip temperature with a time constant of about 1 ms [14]. Both types require special consideration during design and manufacturing process to ensure electrical isolation from HV traces on the substrate and require additional external pins and separate copper traces, which might increase manufacturing cost and give rise to new reliability issues.

Manuscript received September 29, 2014; revised January 23, 2015; accepted March 14, 2015. Date of publication March 31, 2015; date of current version September 29, 2015. This work was supported by the U.K. Engineering and Physical Sciences Research Council through the research Grants EP/I031707/1 and EP/H03014X/1. Recommended for publication by Associate Editor Prof. A. Mertens.

The authors are with the Power Electronics, Machines and Control (PEMC) Group, Department of Electrical and Electronics Engineering, University of Nottingham, Nottingham NG7 2RD, U.K. (e-mail: eexmae@nottingham.ac.uk; mark.johnson@nottingham.ac.uk).

Color versions of one or more of the figures in this paper are available online at <http://ieeexplore.ieee.org>.

Digital Object Identifier 10.1109/TPEL.2015.2418711

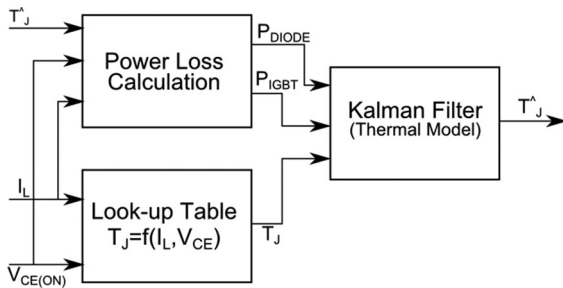


Fig. 1. Block diagram of the complete method for IGBT junction temperature estimation.

In the absence of direct measurements, RC equivalent thermal models can provide a simplified and efficient way to obtain junction temperature estimates for IGBT modules. Reduced order models of the thermal conduction path can be used to get an estimate of junction temperature in real time [15]. However, even with accurate precharacterization of the junction-to-case thermal impedance, large uncertainties in the thermal interfacing and heat sink reduces the applicability of those models [16]. Therefore, thermal characterization of the complete thermal path, by measuring junction-to-ambient thermal impedance, is often needed to achieve more accurate models. Furthermore, these models are generally defined under known boundary condition of a constant ambient or coolant temperature. Any variation in the coolant flow rate results in a variation in the heat transfer coefficient, and consequently, varies the thermal resistance of the heat sink [17]. One solution is a multimodel approach, which considers the effect of variable cooling on the thermal impedance by generating multiple models for multiple cooling rates [18]. This procedure complicates the modeling process and still cannot cope with degradation of the thermal path.

The aging effect of power modules reduces model validity over time, for example, where gradual degradation of the thermal path due to solder fatigue increases thermal resistance [19]. Therefore, adaptive thermal models were proposed to quantify the change in the thermal resistance and update model parameters accordingly [20], [21]. Nonetheless, those models suffer some drawbacks: the method described in [20] requires modification of gate drive to extend the turn-on time of the semiconductor to allow making online measurement of threshold voltage, whereas the method in [21] is intrusive and requires temperature sensors positioned on the baseplate to detect the change of temperature nonuniformity and is highly sensitive to the locations of those sensors.

In this paper, a real-time, noninvasive method to estimate the junction temperature (T_J) of IGBT power modules is proposed, which combines measurements of a temperature sensitive parameter with a thermal model. The approach is shown in Fig. 1 is based on the external measurement of the on-state voltage $V_{CE(ON)}$, at high current, without the need to modify the gate drive circuit or disturb the normal switching cycles of the IGBT. The $V_{CE(ON)}$ measurement is translated into a junction temperature measurement T_J using a look-up table. The resulting T_J measurement can be very noisy due to $V_{CE(ON)}$ measurement

inaccuracies and the low sensitivity of $V_{CE(ON)}$ to temperature. Therefore, a Kalman filter is introduced to improve accuracy and eliminate noise and intermittency in the T_J measurement. The Kalman filter [22] is a model-based approach that uses a thermal model of the heat conduction path to process the T_J measurements resulting from $V_{CE(ON)}$. A power loss model, based on the measured current, is used to calculate power dissipation, which is then used as an input to the Kalman filter. The adaptive property of Kalman filter allows consistent and accurate estimates of junction temperature to be obtained in the presence of aging effects and variable cooling conditions. In addition, examination of the residual error allows the quality of the estimate to be assessed and provides a mechanism for detecting changes in the thermal path. A simulation study of the proposed method was presented previously in [23]. This paper presents the practical implementation and experimental verification of the proposed method for multichip IGBT modules. In Section II, the measurement circuit of $V_{CE(ON)}$ for T_J measurement is presented. Section III introduces the development of the state-space thermal model. Section IV explains the algorithm of Kalman filter. Test setup and experimental results are presented in Section V. Conclusion is in Section VI.

II. USING THERMOSENSITIVE ELECTRICAL PARAMETERS TO ESTIMATE JUNCTION TEMPERATURE

Many recent researches focused on the online measurement of thermosensitive electrical parameters (TSEPs) to resolve temperature information during converter operation. IGBT TSEPs such as on-state voltage $V_{CE(ON)}$ [24], threshold voltage V_{TH} [25], and gate resistance R_G [26] and turn-off timing [27] can be used to estimate junction temperature in real time. Resolving T_J information from TSEPs can be challenging due to the low sensitivity of those TSEPs to T_J and their dependence on the loading conditions of power converters. In addition, the harsh working environment of power modules adds lot of inaccuracies to the measurement. Those inaccuracies originate from the switching and modulation signals and the EMI from the environment, which increases error margins in the resulting T_J measurement [9]. In addition, some TSEPs are affected by the progressive degradation of power modules. For example, on-state voltage $V_{CE(ON)}$ is affected by wire-bond liftoff. The loss of wire-bond shifts up the value of $V_{CE(ON)}$ as a result of electrical resistance increment [28], which can lead to large errors in the measured T_J using that TSEP. In this paper, the on-state voltage $V_{CE(ON)}$ is used to get T_J measurements during normal operation of the power converter.

A. Temperature Dependence of the On-State Voltage $V_{CE(ON)}$

The relationship of $V_{CE(ON)}$ to temperature is dependent on current and has a nonlinear temperature coefficient. Fig. 2 shows the I - V characteristic of 1.2-kV/400-A IGBT module at multiple temperatures, which describes that relationship. It is clear that the temperature coefficient of $V_{CE(ON)}$ is a function of current, where at low currents, $V_{CE(ON)}$ has a negative temperature coefficient, and at high currents, it has a positive temperature coefficient. The point where temperature coefficient changes

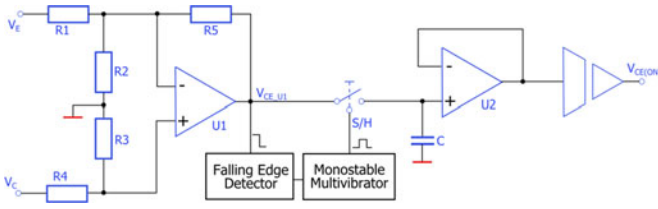


Fig. 2. Schematic of the online measurement circuit of $V_{CE(ON)}$.

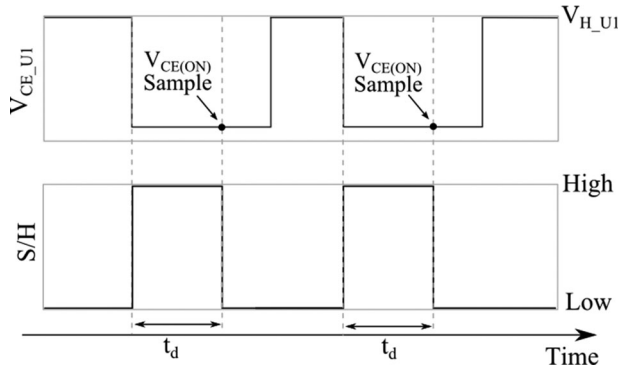


Fig. 3. Operating signals of $V_{CE(ON)}$ measurement circuit. (a) Output of the differential amplifier U1 where V_{H_U1} is the saturation voltage of the op-amp. (b) Sample and hold signal used to capture $V_{CE(ON)}$ value where t_d is delay time between V_{CE} falling edge and sampling instant.

sign is the inflection point and here $V_{CE(ON)}$ becomes independent of temperature. For the example module under test, the negative temperature coefficient of $V_{CE(ON)}$ below inflection point is found to have a maximum value of 1.23 mV/°C at 8 A, which decreases in magnitude toward inflection point. Above that point temperature coefficient becomes positive and increases with current to reach 2.68 mV/°C at 180 A.

B. Online Measurement of the On-State Voltage $V_{CE(ON)}$

Online measurement of the on-state voltage $V_{CE(ON)}$ for temperature measurement, during normal operation of power converters, can be a challenge. The voltage across the IGBT device has a wide dynamic range (between dc-link voltage and on-state voltage) and must be captured with millivolt. Precise timing, synchronized to the device switching instants, is required in order to capture a consistent representation of $V_{CE(ON)}$. In addition, electrical isolation is required between power converter and the processing end point. Therefore, a dedicated measurement circuit is developed to meet these requirements. Fig. 2 shows a schematic of the measurement circuit. The voltage dividers $R1-R2$ and $R3-R4$ scale down V_{CE} voltage to the acceptable range of the U1 inputs. The op-amp U1 is a precision amplifier in a differential configuration. During the off-state of the IGBT V_{CE} voltage equals V_{DC} and the output of the U1 is saturated. However, no measurement is required during IGBT off-state. U1 has a short recovery time so that when the IGBT switches ON, it recovers from saturation and settles to the value of $V_{CE(ON)}$. U1 inputs are protected by ESD diodes against high-voltage spikes. Capacitors in parallel to the resistors $R1-R4$ can be used to improve the frequency response of the voltage dividers if

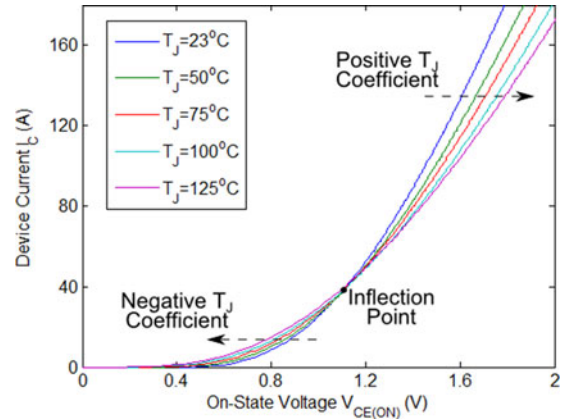


Fig. 4. I - V characteristic of a 1.2-kV/400-A IGBT power module at multiple temperatures explains temperature dependence of the on-state voltage $V_{CE(ON)}$.

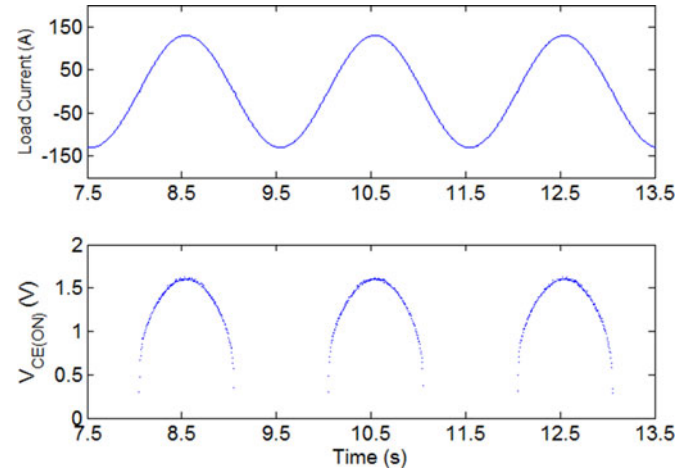


Fig. 5. Online measurement of load current and $V_{CE(ON)}$ during inverter operation.

necessary. The falling edge detector compares the output of U1 with a predefined voltage to detect the falling edge of V_{CE} and triggers the monostable multivibrator to enable the sampling circuit after a 100 μ s of the trigger giving sufficient time for V_{CE} to stabilize. This delay time can be tuned by choosing the appropriate values for the multivibrator components. The capacitive isolation is achieved using an isolation amplifier where the sampled signal is modulated using a high frequency signal and is sent through the isolation barrier (capacitors). It is then demodulated at the other end and the original signal is recovered. A 16-bit analog-to-digital converter (ADC) with a range of ± 5 V is used to acquire $V_{CE(ON)}$ value at the measurement side, which gives a resolution of 0.15 mV.

Every switching cycle, a single sample is captured and held until the next switching cycle. The operation of the circuit is depicted in Fig. 4 where the output of the differential amplifier U1 and the sample and hold signal S/H is shown. The circuit is verified in a full-bridge inverter, where it is connected to the power terminals of the high-side device. Fig. 5 shows the load current signal and the correspondingly measured $V_{CE(ON)}$ signal.

III. DEVELOPMENT OF A STATE-SPACE THERMAL MODEL

Typically, a power module includes a combination of IGBTs and diodes, which form multiple heat sources that contribute to the total heat generation in a module. Fig. 6 shows the half-bridge power module used in this study, where four IGBTs and two free-wheeling diodes are connected in parallel on each substrate tile. The temperature of IGBTs on a single substrate tile is affected by the adjacent diodes on same substrate tile and by the chips on the other substrate tile. In this paper, the cross coupling between diodes and IGBTs on the same substrate tile is considered in the modeling process, whereas the relatively small cross coupling between the two substrate tiles is ignored.

A. Modeling the Self-Heating of the IGBT

The thermal path between the semiconductor chip in a power module and the convective surface of the heat sink consists of a stack of layers of different materials as shown in Fig. 7(a). This thermal path can be characterized by the junction-to-ambient thermal impedance $Z_{\theta_{ja}}(t)$ which is defined as the step response of the junction temperature to a power input. It is described by the ratio of the difference between the junction temperature $T_j(t)$ and a constant ambient temperature T_a to the step power input P_D .

$$Z_{\theta_{ja}}(t) = (T_j(t) - T_a) / P_D. \quad (1)$$

An electrical equivalent RC network can be used to describe this function $Z_{\theta_{ja}}(t)$ with a number of RC elements, forming a Foster network as shown in Fig. 7(b). The time response of the Foster network is described by a series of exponential terms of the following form:

$$Z_{\theta_{ja}}(t) = \sum_{i=1}^n R_i (1 - e^{-t/R_i C_i}). \quad (2)$$

Taking the Laplace transformation of (2) gives the partial fraction expansion form of the transfer function of the thermal impedance in the frequency domain.

$$Z_{\theta_{ja}}(s) = \frac{k_1}{s + p_1} + \frac{k_1}{s + p_1} + \dots + \frac{k_n}{s + p_n} \quad (3)$$

where k_i and p_i are the residues and poles of the transfer function, respectively, and s is the complex variable. By algebraic manipulation, it can be found that poles and residues are related to the RC components by the following formulas:

$$k_i = \frac{1}{C_i}, \quad p_i = \frac{1}{R_i C_i}. \quad (4)$$

It should be noted that these RC elements have no correlation to the physical nature of the thermal path because a Foster network is only a behavioral model of the thermal system [29]. The partial fraction expansion form in (3) can be easily transferred into a state-space model of the parallel form with a diagonal system matrix, where the poles p_i form the elements of the main diagonal while the residues k_i form the elements of the input matrix [30]. The resulting state-space representation for a Foster

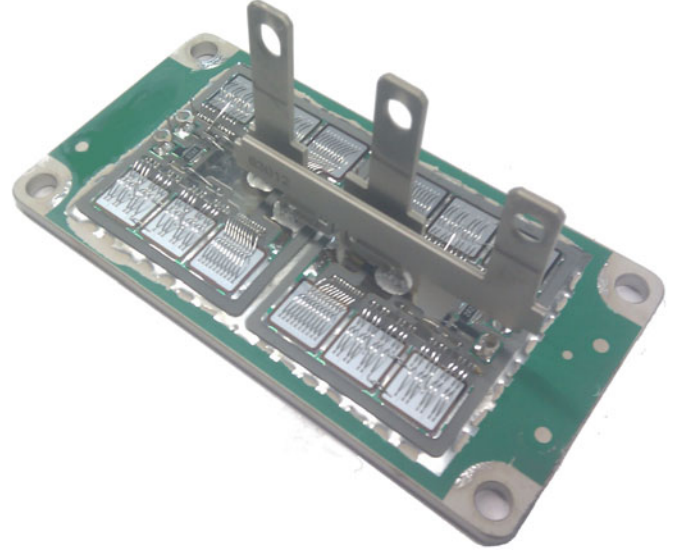


Fig. 6. 1.2-kV/400-A half-bridge power module used in the test. Each substrate tile contains four IGBTs and two freewheeling diodes.

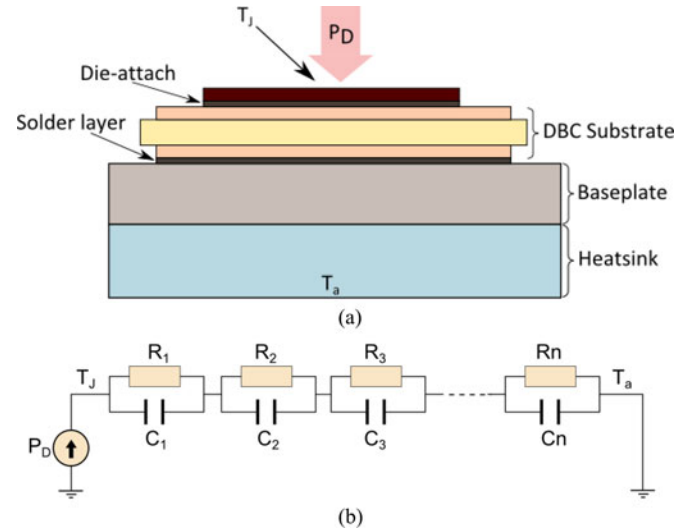


Fig. 7. (a) Multilayered structure of the thermal path of a power module. (b) Electrical equivalent Foster model of a thermal path.

network thermal model is

$$\dot{\mathbf{x}}(t) = \mathbf{A}\mathbf{x}(t) + \mathbf{B}\mathbf{u}(t) \quad (\text{state equation})$$

$$T_j(t) = \mathbf{C}\mathbf{x}(t) + \mathbf{D}\mathbf{u}(t) \quad (\text{output equation})$$

$$\mathbf{A} = \begin{bmatrix} \frac{1}{R_1 C_1} & 0 & 0 & \dots & 0 \\ 0 & \frac{1}{R_2 C_2} & 0 & \dots & 0 \\ 0 & 0 & \frac{1}{R_3 C_3} & \dots & 0 \\ \vdots & \vdots & \vdots & \ddots & \vdots \\ 0 & 0 & 0 & \dots & \frac{1}{R_n C_n} \end{bmatrix} \quad \mathbf{B} = \begin{bmatrix} \frac{1}{C_1} & 0 \\ \frac{1}{C_2} & 0 \\ \frac{1}{C_3} & 0 \\ \vdots & \vdots \\ \frac{1}{C_n} & 0 \end{bmatrix}$$

$$\mathbf{C} = [1 \quad 1 \quad \dots \quad 1] \quad \mathbf{D} = [0 \quad 1] \quad (5)$$

where $A_{n \times n}$ is the system matrix, $B_{n \times 2}$ is the input matrix, $C_{1 \times n}$ is the output matrix, and $D_{1 \times 2}$ is the feed-forward matrix. The state vector $x(t)$ represents the differential temperatures across RC elements, $u(t) = [P_D(t), T_a]$ is the system input vector, where $P_D(t)$ is the power dissipation and T_a is the ambient temperature. The output equation gives the junction temperature $T_J(t)$, which is the total sum of system states and the constant ambient temperature. According to [15], the ambient temperature can be considered additive to the output when the variations in the ambient temperature is slow in comparison to the slowest dynamics in thermal system.

B. Modeling the Diode Cross-Coupling Effect

By accepting negative values of RC components, the Foster network in Fig. 7(b) can be used to model the cross-coupling effect [31]. Therefore, the state-space model in (5) is suitable to represent both the self-heating and cross-coupling thermal impedances individually.

Therefore, an extended model that represents both impedances can be constructed by combining a state-space model of order n for the self-heating impedance with a model of order m for the cross-coupling impedance. This results in a model that describes the thermal behavior of the IGBT dies on one substrate tile. A similar modeling procedure can be used to construct a model for the diode junction temperature. But for simplicity, only the junction temperature of the IGBT is considered here. The complete state-space model description for IGBT junction temperature becomes

$$\begin{aligned} \begin{bmatrix} \dot{x}_{s1} \\ \vdots \\ \dot{x}_{sn} \\ \dot{x}_{c1} \\ \vdots \\ \dot{x}_{cm} \end{bmatrix} &= \begin{bmatrix} p_{s1} & 0 & 0 & 0 & \cdots & 0 \\ 0 & \ddots & 0 & \vdots & \cdots & 0 \\ \vdots & 0 & p_{sn} & 0 & \vdots & 0 \\ 0 & \vdots & 0 & p_{c1} & 0 & \vdots \\ 0 & \cdots & \vdots & 0 & \ddots & 0 \\ 0 & \cdots & 0 & 0 & \cdots & p_{cm} \end{bmatrix} \begin{bmatrix} x_{s1} \\ \vdots \\ x_{sn} \\ x_{c1} \\ \vdots \\ x_{cm} \end{bmatrix} \\ &+ \begin{bmatrix} k_{s1} & 0 & 0 \\ \vdots & \vdots & \vdots \\ k_{s1} & 0 & 0 \\ 0 & k_{s1} & 0 \\ \vdots & \vdots & \vdots \\ 0 & k_{s1} & 0 \end{bmatrix} \begin{bmatrix} P_{IGBT} \\ P_{DIODE} \\ T_a \end{bmatrix} \quad (6) \\ T_J &= [1 \ 1 \ 1 \ \cdots \ 1] \begin{bmatrix} x_{s1} \\ \vdots \\ x_{sn} \\ x_{c1} \\ \vdots \\ x_{cm} \end{bmatrix} + [0 \ 0 \ 1] \begin{bmatrix} P_{IGBT} \\ P_{DIODE} \\ T_a \end{bmatrix} \quad (7) \end{aligned}$$

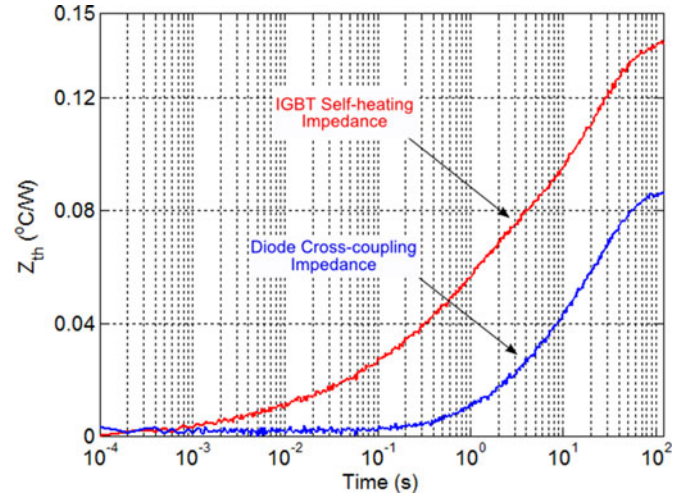


Fig. 8. Measured IGBT module self-heating and cross-coupling thermal impedances.

TABLE I
IDENTIFIED THERMAL MODEL PARAMETERS

Term Num.		1	2	3	4
Self-Heating	R_i	0.0126	0.0265	0.034	0.0669
	C_i	0.4075	7.284	51.054	363.93
Cross coupling	R_i	0.0320	-0.032	0.0199	0.066
	C_i	6.8947	-8.013	112.58	346.91

where x_{s1}, \dots, x_{sn} are the states of the self-heating impedance, and p_{s1}, \dots, p_{sn} and k_{s1}, \dots, k_{sn} are the poles and residues of the self-heating impedance, respectively. Similarly, x_{c1}, \dots, x_{cm} are the states of the cross-coupling impedance, whereas p_{c1}, \dots, p_{cm} and k_{c1}, \dots, k_{cm} are the poles and residues of the self-heating impedance, respectively. T_J is the IGBT junction temperature. T_a is the ambient temperature, P_{IGBT} and P_{Diode} are the power dissipation of the IGBT and diode, respectively.

C. Identification of Model Parameters

Fig. 8 shows the measured self-heating and cross-coupling junction-to-ambient thermal impedance curves for one side of the half-bridge module. Thermal impedance curves were obtained by measuring the cooling curve of the IGBT using the voltage drop V_{CE} across the IGBT at a current of 40 mA as a TSEP. A calibrated relationship $T_J = f(V_{CE})$ is then used to convert the voltage into a temperature measurement. The thermal propagation time which is the time necessary for the heat generated by the diodes to reach the adjacent IGBTs is about 0.1 s as it is seen on the diode cross-coupling impedance.

It is found that a fourth order model is a good approximation for both self-heating and cross-coupling impedances. By least-square fitting of (2) to the measured data shown in Fig. 8, the RC component values are determined. The resulting fitting parameters are shown in Table I.

IV. FORMULATION OF KALMAN FILTER

A Kalman filter is a model-based state estimator, which estimates the temperature of an IGBT utilizing a linear model of thermal path given inaccurate power dissipation as an input and an inaccurate measurement of junction temperature. The continuous state-space model in (6) is first discretized with a time step t_s using the Euler backward method, resulting in a discrete state-space model with a time step k and F and G as the state transition matrix and input matrix respectively. Then, a process noise w_k and a measurement noise v_k are added to the model to account for inaccuracies in modeling, power dissipation, and measurement signal. Noise terms are assumed to be uncorrelated white Gaussian noise with known covariances Q and R for process and measurement noise, respectively, whereas H is the process noise gain matrix. The resulting discrete model is written as

$$\mathbf{x}_k = \mathbf{F}\mathbf{x}_{k-1} + \mathbf{G}\mathbf{u}_k + \mathbf{H}w_k \quad (8)$$

$$T_k = \mathbf{C}\mathbf{x}_k + \mathbf{D}\mathbf{u}_k + v_k. \quad (9)$$

The Kalman filter works in two recursive predict-correct steps in order to minimize the mean squared error of the estimate. In the prediction step, the model is used to calculate the predicted states \hat{x}_k^- using the present calculated power dissipation \mathbf{u}_k and the corrected states \hat{x}_{k-1}^+ from the previous step. The predicted error covariance P_k^- is calculated as well. When a measurement T_k becomes available, the correction step is implemented and the residual e_k is obtained by the difference between the measurement T_k and the estimate \hat{T}_k^- . The corrected state \hat{x}_k^+ is calculated by updating the predicted state with the residual e_k using the calculated Kalman gain matrix K_k . This process is depicted by the following relationships, which explain the recursive implementation of algorithm.

Predict

$$\hat{\mathbf{x}}_k^- = \mathbf{F}\hat{\mathbf{x}}_{k-1}^+ + \mathbf{B}\mathbf{u}_k \quad (10)$$

$$\hat{T}_k^- = \mathbf{C}\hat{\mathbf{x}}_k^- + \mathbf{D}\mathbf{u}_k \quad (11)$$

$$\mathbf{P}_k^- = \mathbf{F}\mathbf{P}_{k-1}^+ \mathbf{F}^T + \mathbf{H}\mathbf{Q}\mathbf{H} \quad (12)$$

Correct

$$e_k = T_k - \hat{T}_k^- \quad (13)$$

$$\mathbf{K}_k = \mathbf{P}_k^- \mathbf{C} [\mathbf{C}\mathbf{P}_k^- \mathbf{C}^T + R]^{-1} \quad (14)$$

$$\hat{\mathbf{x}}_k^+ = \hat{\mathbf{x}}_k^- + a\mathbf{K}_k e_k \quad (15)$$

$$\mathbf{P}_k^+ = [\mathbf{I} - \mathbf{K}_k \mathbf{C}] \mathbf{P}_k^- \quad (16)$$

The filter is tuned by varying Q and R to get the best performance [22]. The parameter a in (15) takes the value 1 when a measurement T_k is available otherwise it takes the value 0. That makes the corrected state \hat{x}_k^+ equal to the predicted state \hat{x}_k^- and ensures the continuity of the estimate in the absence of the measurement, which is the case when the IGBT is not conducting. In other words, during the availability of the T_k measurement both predict and correct steps are implemented, otherwise only the predict step is carried out as depicted in Fig. 9.

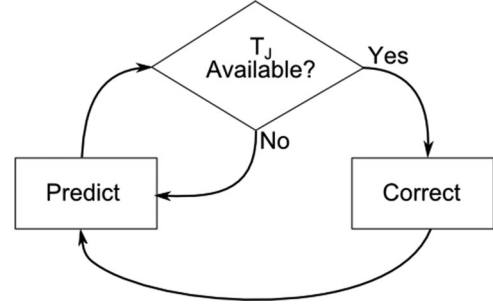


Fig. 9. Sequence of Kalman filter predict and correct steps is dependent of the availability of T_k measurement.

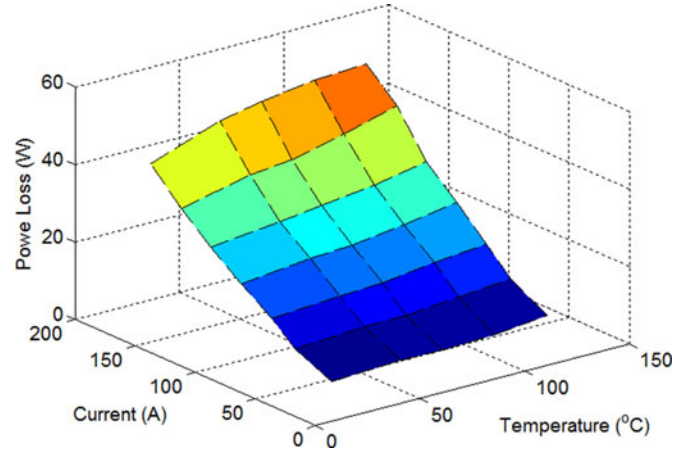


Fig. 10. Switching power loss model of the IGBT at $V_{DC} = 100$ V.

A. Power Loss Calculation

Kalman filter requires an input of the IGBT and diode power dissipation. The total power dissipation of the IGBT P_{IGBT} is the summation of conduction loss P_{cond} and switching loss P_{sw} , where the conduction loss is calculated by the multiplication of loading current I_L and the on-state voltage $V_{CE(ON)}$. The switching loss consists of turn-on and turn-off losses represented by E_{on} and E_{off} , respectively, and f_{sw} is the switching frequency [32]. The power loss is calculated according to the following formulas:

$$P_{IGBT} = P_{cond} + P_{sw} \quad (17)$$

$$P_{cond} = V_{CE(ON)} \times I_L \quad (18)$$

$$P_{sw} = (E_{on} + E_{off}) \times f_{sw}. \quad (19)$$

A look-up table is used to calculate the switching losses, utilizing the load current, dc-link voltage V_{DC} , and the junction temperature. Fig. 10 shows the look-up table for the IGBT switching losses P_{sw} at a constant $V_{DC} = 100$ V. Similarly, the power dissipation of the diode P_{DIODE} , consisting of conduction loss and reverse recovery loss, is calculated using another look-up table.

B. T_J Measurement Signal

The measurement of T_J obtained from $V_{CE(ON)}$ constitutes the measurement signal of Kalman filter. This measurement as

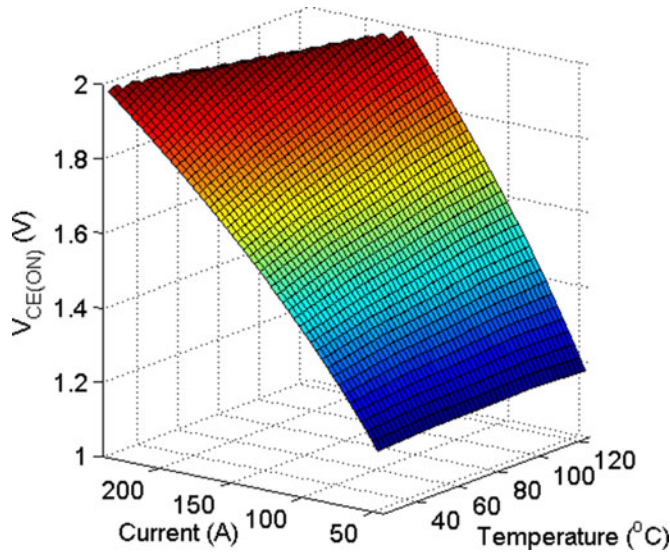


Fig. 11. Look-up table used to get T_J using measurement of $V_{CE(ON)}$ and current.

explained in Section II can be informative only above a certain current level [24]. Therefore, the measurement signal becomes intermittent if current level varies over a wide range as is typical in an inverter. A look-up table is used to replicate the I - V characteristic of the IGBT. The data for the look-up table are collected by a curve tracer and the realization of the look-up table is shown in Fig. 11. It is this look-up table used to obtain T_J measurement utilizing the measurement circuit explained in Section II.

V. EXPERIMENTAL VERIFICATION

Experimental verification of the algorithm is performed on a full-bridge inverter with the junction temperature of the high-side IGBT in one half bridge. The system utilizes two 1.2-kV/400-A half-bridge IGBT power modules. The modules are uncovered and sprayed in black to allow thermal imaging with an infrared camera for verification. The modules are fixed on a copper water cooled heat sink and are connected to an inductive load of 300 μ H. A current transducer is used to measure the load current and the on-state voltage is measured using the circuit described in Section II, which is connected to the power terminals of the high side IGBT. The measurement circuit is connected to a dSPACE digital system, which utilizes a 16-bit ADC with a range of ± 5 V provides a resolution of 0.1 mV for $V_{CE(ON)}$ measurement. The load current is controlled by a PI current controller, which, along with the Kalman filter and PWM generator, is implemented on the dSPACE system. A unipolar switching scheme is used to generate a 3-kHz PWM switching signals taking into consideration the blanking time required to prevent short circuiting of upper and lower devices, which is about $t_B = 0.1 \mu$ s. A combination of optical and capacitive isolation ensures a complete electrical isolation between the inverter and the digital system. The inverter test rig is shown in Fig. 12 and a block diagram of the setup is shown in Fig. 13.

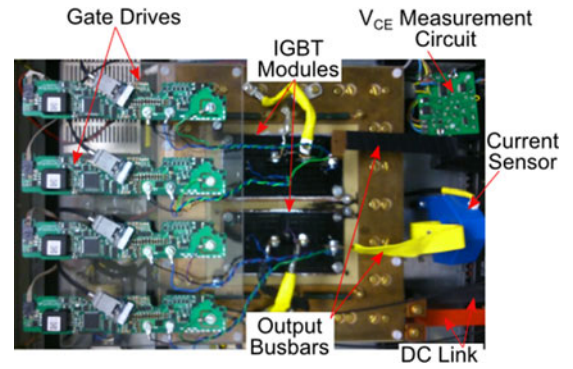


Fig. 12. Image of the full-bridge inverter showing the power modules, gate drives, current sensor, and $V_{CE(ON)}$ measurement circuit.

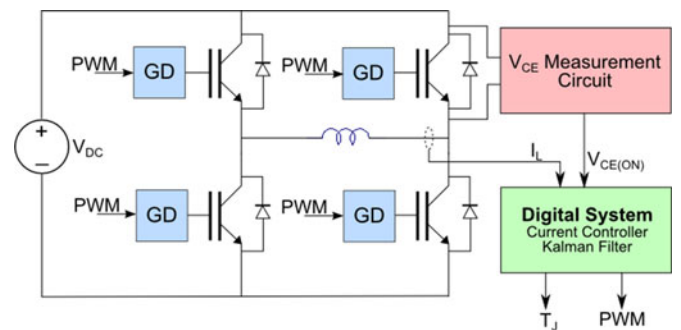


Fig. 13. Block diagram of the experimental setup used for algorithm verification. A full-bridge inverter is controlled by a digital system.

For experimental verification of junction temperature estimate, it is necessary to understand the representative temperature estimated by $V_{CE(ON)}$. In [33], it is found that the temperature measured by the voltage drop V_{CE} represents a weighted average of chip temperatures where the weighting vector is proportional to the current density such that areas on the chip with the highest current density and highest temperature dominate the measurement of V_{CE} . Similarly, in [34], it is reported that the voltage drop across multiple paralleled IGBTs operating at different temperatures is a temperature weighted average with the hottest chip being the most influential.

Therefore, the maximum temperature among the monitored IGBTs is selected for comparison. An infrared camera with an accuracy of ± 1 $^{\circ}$ C and a sampling frequency of 50 Hz is used to measure the temperature at the top surface of the IGBTs during inverter operation. Fig. 14 shows the thermal image of the monitored IGBTs of the high side of one leg in the inverter. The maximum temperature on each chip is found by examining the temperature profile across the chip diagonal, and then, the maximum temperature among the chips is chosen for comparison.

A. Verification of T_J Measurement Obtained From $V_{CE(ON)}$

As explained in the previous section, the measurement of $V_{CE(ON)}$ can be translated into a measurement of T_J utilizing a look-up table and the load current. Fig. 15 shows the measurement of T_J obtained from the on-state voltage $V_{CE(ON)}$

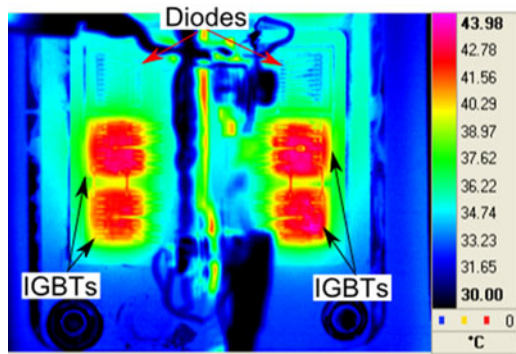


Fig. 14. Thermal image of the high-side IGBT during inverter operation.

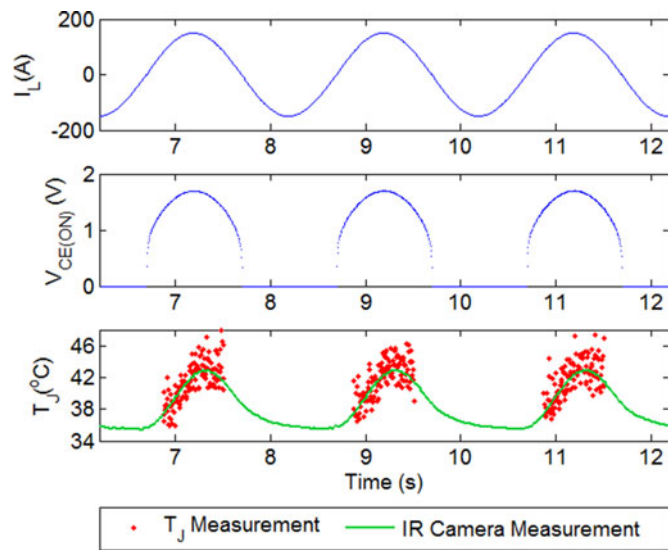


Fig. 15. Online measurements of load current I_L , $V_{CE(ON)}$, and T_J measurement compared to IR camera measurement.

compared to the IR camera measurement along with the corresponding sinusoidal load current and on-state voltage. It is obvious that T_J measurement has a large spread due to measurement noise inherited from $V_{CE(ON)}$, which is estimated to be 14 mVpp. The intermittency that disturbs the continuity of the T_J measurement signal in comparison to IR measurement happens when the current changes direction and when the current value goes below a specific limit, in this case, about 80 A.

B. Verification of Kalman Filter Estimate of Junction Temperature

Fig. 16(a) shows the T_J estimate given by the Kalman filter in comparison to the IR camera measurement and the T_J measurement obtained from $V_{CE(ON)}$. It is evident that the estimate of T_J given by the Kalman filter tracks the IR camera measurement accurately during both heating and cooling regimes with a maximum error of 3.4%. The error between the T_J estimate and the IR camera measurement is shown in Fig. 16(b). The difference between the two signals at the peaks of temperature

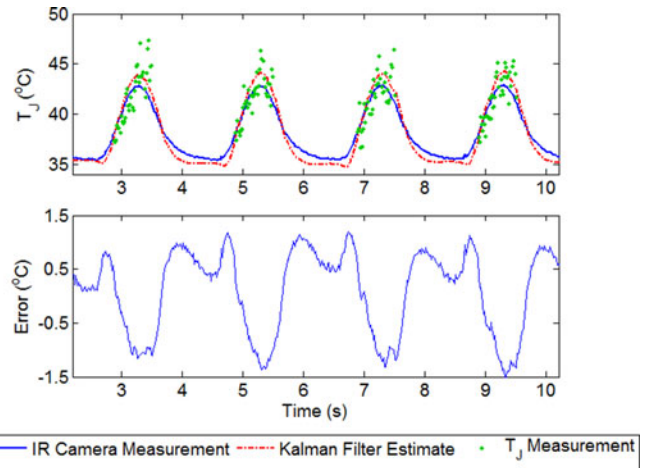


Fig. 16. (a) Kalman estimate of junction temperature compared to IR camera measurement and T_J measurement by $V_{CE(ON)}$. (b) Difference between IR camera measurement and T_J estimate.

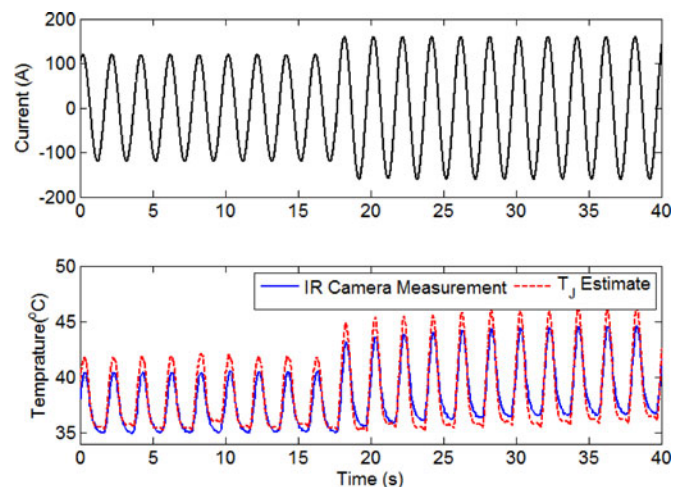


Fig. 17. IR camera measurement and T_J estimate when current amplitude is changed from 120 to 160 A as can be seen in the load current.

profile which is about 1.3 °C can be attributed to many factors. First, the IR camera measures the temperature at the top surface of the IGBT, whereas $V_{CE(ON)}$ indicates the temperature at the intrinsic body region buried inside the IGBT. Second, the presence of the wire-bonds on the top of the chip prevents the IR camera from obtaining the maximum temperature due to the shading effect and the measured temperature could, therefore, be lower than reality [35]. In addition, calibration of look-up table is done under isothermal conditions, while in practice, there are temperature gradients across the module. Since $V_{CE(ON)}$ is measured across the power terminals, the measurement includes the voltage drop across the packaging resistance, which is affected by temperature gradients. This results in a mismatch with the calibration. On the other hand, the difference between IR camera and T_J estimate in the cooling regime, which shows a maximum of 1.5 °C, is justified by the fact that no $V_{CE(ON)}$ data are available for T_J measurement and the correction step of the Kalman filter implementation is not carried out. As a result,

TABLE II
ERROR STATISTICS OF T_J MEASUREMENT AND T_J ESTIMATE

	Mean Absolute Error (°C)	Standard Deviation(°C)
T_J measurement by $V_{CE(ON)}$	1.40	2.06
T_J estimate	0.74	0.62

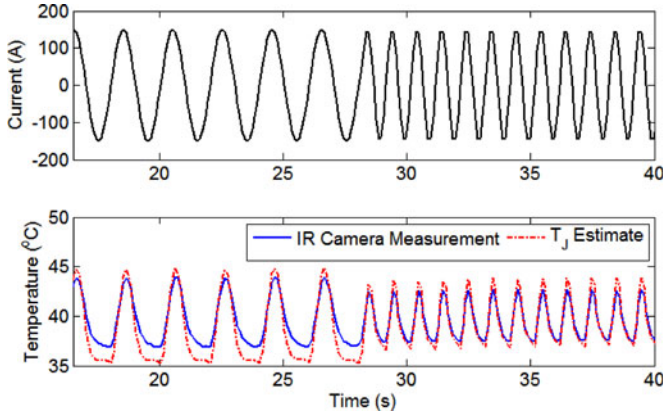


Fig. 18. IR camera measurement and T_J estimate when modulation frequency is changed from 0.5 to 1 Hz as can be seen in the load current.

the estimate in this regime is purely dependent on the thermal model. The difference is then linked to errors inherited from the modeling process.

Compared to the T_J measurement, the estimate is noise free and continuity of the signal is preserved. To evaluate the improvement in the T_J estimate over the T_J measurement, the mean absolute error (MAE) and standard deviation (σ) of the error is examined. The errors of the T_J estimate and the T_J measurement are acquired by subtracting the T_J estimate and the T_J measurement from the IR camera measurement. Table II shows the statistics of the two error signals. It is evident that the accuracy of T_J estimate has improved compared to T_J measurement obtained by $V_{CE(ON)}$ with 53% less MAE and 30% less spread.

Inverter modulation frequency and amplitude both affect the junction temperature response. To demonstrate the consistency of the T_J estimate under variable operating conditions, the load current is varied in the inverter. Fig. 18 shows the T_J estimate response at the instant when the modulation frequency changes from 0.5 to 1 Hz with constant amplitude 150 A. The agreement of the T_J estimate with the IR camera measurements is maintained. It is seen that the ripple ΔT in T_J is reduced when the frequency is increased whereas the mean temperature T_m is nearly constant in agreement with IR camera measurement as can be seen in Table III. This is to be expected since the frequency response of the thermal system replicates a low-pass filter.

Fig. 17 shows T_J estimate when current amplitude is increased from 120 to 160 A with a modulation frequency of 0.5 Hz. The increment in the mean temperature and the ripple is evident in Table IV for both IR measurement and T_J estimate.

TABLE III
 T_J PROFILE PARAMETERS FOR IR CAMERA AND T_J ESTIMATE UNDER A CHANGE IN MODULATION FREQUENCY

	0.5 Hz		1 Hz	
	IR Camera	T_J Estimate	IR Camera	T_J Estimate
T_m	40.43	40.13	40.1	40.47
ΔT	6.9	9.2	4.96	6.79

TABLE IV
 T_J PROFILE PARAMETERS FOR IR CAMERA AND T_J ESTIMATE UNDER A CHANGE IN CURRENT AMPLITUDE

	120 A		160 A	
	IR Camera	T_J Estimate	IR Camera	T_J Estimate
T_m	37.68	38.55	40.51	41.01
ΔT	5.49	6.65	7.89	10.29

C. T_J Estimate Under Unstable Boundary Condition

As discussed before, large variations in heat transfer coefficient can result from deviations of coolant flow rate. For examination of these effects on the T_J estimate, the water flow in the heat sink is blocked completely by switching the water pump OFF during inverter operation. Water blockage prevents heat removal by convection at the baseplate and increases the thermal resistance of the heat sink [17]. Fig. 19(a) shows the T_J estimate compared to the IR camera measurement along with the baseplate temperature T_C in Fig. 19(b) when the water pump is stopped after reaching thermal equilibrium. The baseplate temperature T_C is measured with a thermocouple fixed to the back side of the baseplate facing the coolant. The water pump is stopped for 84 s, where upon the peak junction, temperature increases from 42 to 58 °C, whereas the baseplate temperature increases correspondingly from 32 to 43 °C. The pump is turned ON again and T_J goes down back to 43 °C after 52 s in good agreement with IR camera measurement, whereas T_C falls back to 32 °C.

The difference between the IR camera measurements and the T_J estimate is shown in Fig. 19(c). A gradual increment in error margins during the transient state with a slight shift in the mean value can be clearly seen. However, regardless of the growing error, which remains within 3.6%, the adaptive property of Kalman filter preserves estimate consistency and robustness by the predict-correct mechanism. The T_J measurement derived from $V_{CE(ON)}$ is utilized to update the T_J estimate and keep it in track with the true value obtained from the IR camera as can be seen from Fig. 19(a).

D. Detecting Thermal Resistance Change Using the Residual Signal

The growing error in Fig. 19(c) is justified by the degraded performance of the Kalman filter due to changes in the thermal model parameters. As water flow rate is brought down to zero, the convective coefficient of heat transfer in the heat sink

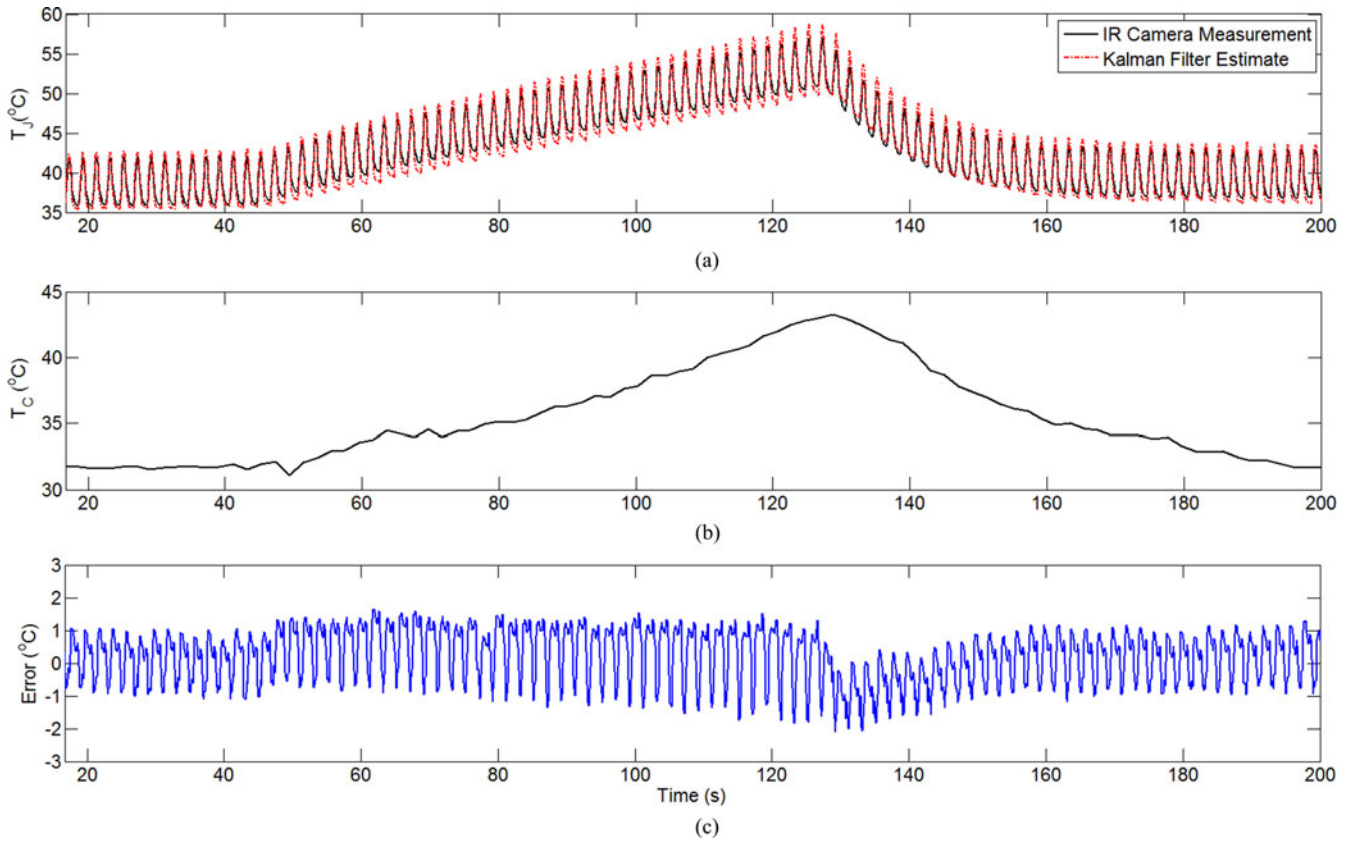


Fig. 19. (a) IR camera measurement and T_J estimate over the duration of water flow blockage. (b) Corresponding baseplate temperature T_C . (c) Difference between IR camera measurement and T_J estimate.

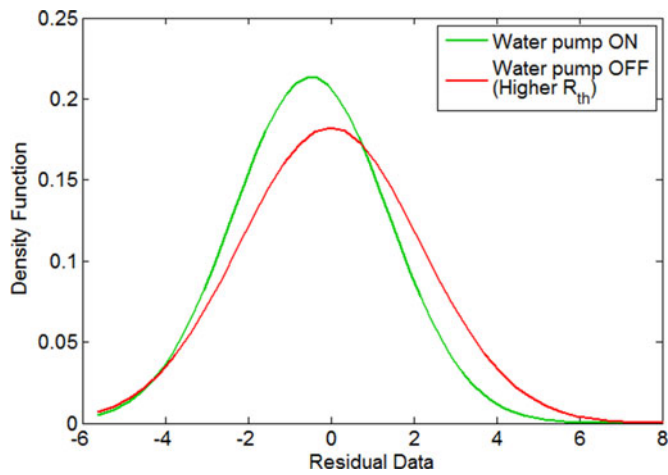


Fig. 20. Statistical distribution of the residual clearly indicates a change in thermal system parameters as R_{th} increases after water pump is stopped.

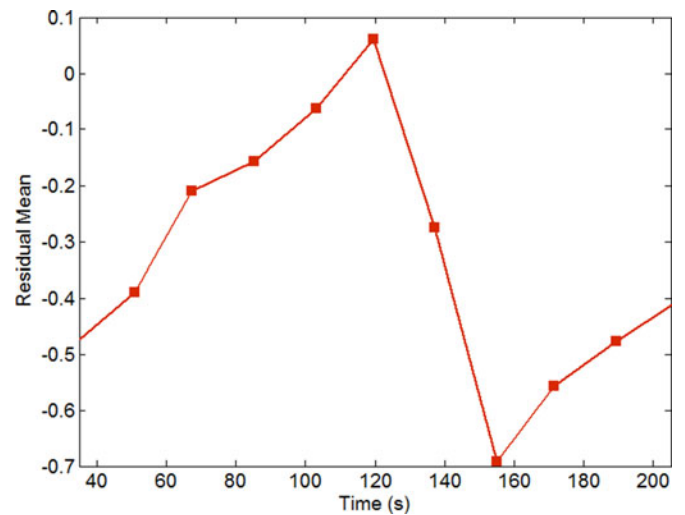


Fig. 21. Time evolution of the mean value of the residual follows the direction of the change in thermal resistance. This can be used as a failure indicator for thermal path degradation.

decreases, which increases the thermal resistance of the heat sink. As a consequence, the junction-to-ambient thermal impedance modeled by the RC network is no longer valid. The degraded performance can be quantified by the examination of the estimate residual produced by the Kalman filter [36], where the residual is the difference between the T_J estimate and the T_J measurement derived from $V_{CE(ON)}$. Fig. 20 shows the statistical distribution of the normalized residual before

and after the pump shutdown. It is evident that the statistical distribution of the residual exhibits a change when the thermal system is altered. Fig. 21 shows the time evolution of residual mean value, which ramps up from -0.515 to 0.06 following the change in the thermal resistance of the heat sink, and then, falls back to its original value when water flows again in

the heat sink. The initial value of the residual mean -0.515 indicates an initial mismatch between the thermal model and the real thermal path, which can be a result of modeling errors. The negative sign indicates that the model underestimates the junction temperature, which is corrected by the Kalman filter.

Degradation of the thermal path increases the residual mean indicating an increased thermal resistance. This correlation between the residual mean and the thermal resistance enables using the residual as a failure indicator of the thermal path. It allows monitoring the state of the thermal path to detect any increment in thermal resistance that might result from solder fatigue. Residual evaluation can be achieved by statistical classification and machine learning methods. Learning the behavior of the residual signal under different healthy and faulty conditions can enable the decision-making process about an ongoing degradation, which can trigger an alarm indicating a potential failure. It is important for the residual evaluation method to provide a reliable and fast detection of any deviation in the residual from its healthy conditions.

Since the residual signal is indicative of a mismatch between the thermal model and the measurement different reasons can cause it to deviate from its original characteristic: a change in the thermal impedance $Z_{\theta ja}$ or a change in the measurement signal of $V_{CE(ON)}$ due to measurement circuit malfunction or wire-bond liftoff.

Wire-bond liftoffs can lead to wrong estimate of T_J since $V_{CE(ON)}$ will deviate from its normal value as a result of wire-bond liftoff. However, this can still be detected by the evaluation of the residual signal. Alternatively, an alternative TSEP, which is not affected by wire-bond liftoffs such as threshold voltage (V_{th}) can be used instead of $V_{CE(ON)}$. Nevertheless, it is required to obtain more measurements from the IGBT in order to enable more efficient diagnosis of system failures and identify the true reason behind a change in residual characteristic.

VI. CONCLUSION

The instantaneous junction temperature of an IGBT power module is estimated in real time. Online measurements of the on-state voltage $V_{CE(ON)}$, obtained at high current during normal operation of power converter, are used as a TSEP to get a measurement of T_J . No modification of the control strategy of the power converter is necessary to make the measurement. A Kalman filter is then applied to the resulting T_J measurement to reduce noise and eliminate the effects of intermittency of the $V_{CE(ON)}$ measurement by constraining the measurement signal to a thermal model in a predict-correct manner. A state-space representation of the thermal model is developed to derive a Kalman filter utilizing the junction-to-ambient thermal impedance measurement of IGBT self-heating and diode cross coupling. The proposed method is implemented on a full-bridge inverter and is verified with an IR camera measurement of the IGBT module during normal operation of the inverter. Excellent matching is achieved between the T_J estimate and the IR camera measurement under different loading and cooling conditions, demonstrating the ability of the method to adapt to variations in the operating conditions of power converter. An

improved accuracy is obtained by the Kalman filter compared to T_J measurement obtained by $V_{CE(ON)}$ alone. The use of the residual signal to detect a change in the thermal resistance is demonstrated, which offers a potential means to monitor the gradual degradation in the thermal path, for example, due to solder fatigue. This method can form part of a real-time health management or active control system for power converters and can be easily integrated within existing power converter control elements.

REFERENCES

- [1] O. V. R. John and R. Bayerer, "High temperature power electronics IGBT modules for electrical and hybrid vehicles," in *Proc. Int. Microelectron. Packag. Soc. High Temp. Electron. Netw.*, Oxford, U.K., 2009, pp. 199–204.
- [2] R. Pittini, S. D'Arco, M. Hernes, and A. Petterteig, "Thermal stress analysis of IGBT modules in VSCs for PMSG in large offshore wind energy conversion systems," in *Proc. 14th Eur. Conf. Power Electron. Appl.*, 2011, pp. 1–10.
- [3] H. Hui and P. A. Mawby, "A lifetime estimation technique for voltage source inverters," *IEEE Trans. Power Electron.*, vol. 28, no. 8, pp. 4113–4119, Aug. 2013.
- [4] M. Musallam, C. M. Johnson, Y. Chunyan, L. Hua, and C. Bailey, "In-service life consumption estimation in power modules," in *Proc. 13th Power Electron. Motion Control Conf.*, 2008, pp. 76–83.
- [5] M. Weckert and J. Roth-Stielow, "Chances and limits of a thermal control for a three-phase voltage source inverter in traction applications using permanent magnet synchronous or induction machines," in *Proc. 14th Eur. Conf. Power Electron. Appl.*, 2011, pp. 1–10.
- [6] M. Musallam, P. P. Acarnley, C. M. Johnson, L. Pritchard, and V. Pickert, "Estimation and control of power electronic device temperature during operation with variable conducting current," *IET Circuits, Devices Syst.*, vol. 1, pp. 111–116, 2007.
- [7] D. A. Murdock, J. E. Ramos, J. J. Connors, and R. D. Lorenz, "Active thermal control of power electronics modules," in *Proc. 38th IAS Annu. Meeting Conf. Rec. Ind. Appl. Conf.*, 2003, vol. 3, pp. 1511–1515.
- [8] A. Castellazzi, W. J. Choy, and P. Zanchetta, "Dynamic active cooling for improved power system reliability," *Microelectron. Rel.*, vol. 51, pp. 1964–1967, 2011.
- [9] N. Baker, M. Liserre, L. Dupont, and Y. Avenas, "Junction temperature measurements via thermo-sensitive electrical parameters and their application to condition monitoring and active thermal control of power converters," in *Proc. 39th Annu. Conf. IEEE Ind. Electron. Soc.*, 2013, pp. 942–948.
- [10] S. Yang, D. Xiang, A. Bryant, P. Mawby, L. Ran, and P. Tavner, "Condition monitoring for device reliability in power electronic converters: A review," *IEEE Trans. Power Electron.*, vol. 25, no. 11, pp. 2734–2752, Nov. 2010.
- [11] N. Patil, J. Celaya, D. Das, K. Goebel, and M. Pecht, "Precursor parameter identification for insulated gate bipolar transistor (IGBT) prognostics," *IEEE Trans. Rel.*, vol. 58, no. 2, pp. 271–276, Jun. 2009.
- [12] N. Patil, D. Das, and M. Pecht, "A prognostic approach for non-punch through and field stop IGBTs," *Microelectron. Rel.*, vol. 52, pp. 482–488, 2012.
- [13] A. Zanin, *SKiM IGBT Modules Technical Explanations*, Semikron, Nuremberg, Germany, 2013.
- [14] D. Domes and U. Schwarzer, "IGBT-module integrated current and temperature sense features based on sigma-delta converter," presented at the Power Conversion Intelligent Motion Eur., Nuremberg, Germany, 2009.
- [15] M. Musallam and C. M. Johnson, "Real-time compact thermal models for health management of power electronics," *IEEE Trans. Power Electron.*, vol. 25, no. 6, pp. 1416–1425, Jun. 2010.
- [16] R. Schnell, M. Bayer, and S. Geissmann, "Thermal design and temperature ratings of IGBT modules," ABB Application Note 5SYA 2093, 2013.
- [17] O. Karim, J. C. Crebier, C. Gillot, C. Schaeffer, B. Mallet, and E. Gimet, "Heat transfer coefficient for water cooled heat sink: Application for standard power modules cooling at high temperature," in *Proc. IEEE 32nd Annu. Power Electron. Spec. Conf.*, 2001, vol. 4, pp. 1938–1943.
- [18] G. C. James, V. Pickert, and M. Cade, "A thermal model for a multichip device with changing cooling conditions," in *Proc. 4th IET Conf. Power Electron., Mach. Drives*, 2008, pp. 310–314.

- [19] A. J. Yerman, J. F. Burgess, R. O. Carlson, and C. A. Neugebauer, "Hot spots caused by voids and cracks in the chip mountdown medium in power semiconductor packaging," *IEEE Trans. Compon., Hybrids, Manuf. Technol.*, vol. CHMT-6, no. 4, pp. 473–479, Dec. 1983.
- [20] C. Hui Feng, J. Bing, V. Pickert, and C. Wenping, "Real-time temperature estimation for power MOSFETs considering thermal aging effects," *IEEE Trans. Device Mater. Rel.*, vol. 14, no. 1, pp. 220–228, Mar. 2014.
- [21] W. Ze, Q. Wei, T. Bo, and Q. Liyan, "An effective heat propagation path-based online adaptive thermal model for IGBT modules," in *Proc. IEEE 29th Annu. Appl. Power Electron. Conf. Expo.*, 2014, pp. 513–518.
- [22] M. S. Grewal and A. P. Andrews, *Kalman Filtering: Theory and Practice Using MATLAB*. New York, NY, USA: Wiley, 2011.
- [23] M. A. Eleffendi and C. M. Johnson, "Thermal path integrity monitoring for IGBT power electronics modules," in *Proc. 8th Int. Conf. Integr. Power Syst. (CIPS)*, 2014, pp. 1–7.
- [24] K. Yong-Seok and S. Seung-Ki, "On-line estimation of IGBT junction temperature using on-state voltage drop," in *Proc. IEEE Ind. Appl. Conf. 33rd IAS Annu. Meeting*, 1998, vol. 2, pp. 853–859.
- [25] I. Bahun, Č. Neven, and Ž. Jakopović, "Real-time measurement of IGBTs operating temperature," *Automatika: J. Control, Meas., Electron.*, vol. 52, pp. 295–305, 2011.
- [26] W. Brekel, T. Duetemeyer, G. Puk, and O. Schilling, "Time resolved in situ T_{vj} measurements of 6.5 kV IGBTs during inverter operation," presented at the Power Conversion Intelligent Motion Eur., Nuremberg, Germany, 2009.
- [27] V. Sundaramoorthy, E. Bianda, R. Bloch, I. Nistor, G. Knapp, and A. Heinemann, "Online estimation of IGBT junction temperature (T_j) using gate-emitter voltage (V_{ge}) at turn-off," in *Proc. 15th Eur. Conf. Power Electron. Appl.*, 2013, pp. 1–10.
- [28] M. Held, P. Jacob, G. Nicoletti, P. Scacco, and M. H. Poech, "Fast power cycling test of IGBT modules in traction application," in *Proc. Int. Conf. Power Electron. Drive Syst.*, 1997, vol. 1, pp. 425–430.
- [29] P. Nance and M. März, "Thermal modeling of power-electronic systems," Infineon Technologies Application Note 05/2000, 2000.
- [30] N. S. Nise, *Control Systems Engineering*. New York, NY, USA: Wiley, 2011.
- [31] M. J. Whitehead and C. M. Johnson, "Determination of thermal cross-coupling effects in multi-device power electronic modules," in *Proc. 3rd IET Int. Conf. Power Electron., Mach. Drives*, 2006, pp. 261–265.
- [32] N. Mohan, T. M. Undeland, and W. P. Robbins, *Power Electronics: Converters, Applications, and Design*. New York, NY, USA: Wiley, 2003.
- [33] R. Schmidt and U. Scheuermann, "Using the chip as a temperature sensor—The influence of steep lateral temperature gradients on the $V_{ce}(T)$ -measurement," in *Proc. 13th Eur. Conf. Power Electron. Appl.*, 2009, pp. 1–9.
- [34] E. Farjah and R. Perret, "Application and analysis of thermosensitive parameters in the case of hybrid power modules," in *Proc. IEEE Ind. Appl. Soc. Annu. Meeting*, 1994, vol. 2, pp. 1284–1289.
- [35] T. Bruckner and S. Bernet, "Estimation and measurement of junction temperatures in a three-level voltage source converter," *IEEE Trans. Power Electron.*, vol. 22, no. 1, pp. 3–12, Jan. 2007.
- [36] R. K. Mehra and J. Peschon, "An innovations approach to fault detection and diagnosis in dynamic systems," *Automatica*, vol. 7, pp. 637–640, 1971.



Mohd. Amir Eleffendi received the B.Sc. degree in computer engineering from the University of Aleppo, Aleppo, Syria and the M.Sc. degree in control systems from the University of Sheffield, Sheffield, U.K., in 2011. Since 2012, he has been working toward the Ph.D. degree at the University Of Nottingham, Nottingham, U.K., where he is currently researching prognostics and health management for power electronics.

In 2011, he joined the University Technology Center, University of Sheffield, as a Research Assistant, where he worked on Fault Detection and Diagnosis. His research interests include thermal management and modeling, thermosensitive electrical parameters, signal processing, health monitoring, and fault-diagnosis algorithms.



C. Mark Johnson (M' 1990) received the B.A. degree in engineering and the Ph.D. degree in electrical engineering from the University of Cambridge, Cambridge, U.K., in 1986 and 1991, respectively.

From 1990 to 1992, he was a Research Associate at the University of Cambridge, and in 1992, he joined as a Lecturer the University of Newcastle, Callaghan, U.K., where his research included the design, analysis, and characterization of power semiconductor devices, resonant power conversion, and instrumentation. From 1998 to 2001, he managed the U.K. national programme on Silicon Carbide electronics, and in 2000, he became a Reader of power electronics at the University of Newcastle. In 2003, he was appointed as the Rolls-Royce/RAEng Research Professor of power electronic systems at the University of Sheffield, and in 2006, he was appointed to a personal chair at the University of Nottingham, where he leads research into power semiconductor devices, power device packaging, reliability, thermal management, power module technologies, and power electronic applications. He is the Director of the U.K. Engineering and Physical Sciences Research Council Centre for Power Electronics, which combines the UK's best academic talent to address the key research challenges underpinning power electronics, and is a member of the Executive for the U.K. Innovative Electronics Manufacturing Research Centre.